J. Appl. Comput. Mech., 6(4) (2020) 934-955
DOI: 10.22055/JACM.2019.29781.1637

ISSN: 2383-4536
jacm.scu.ac.ir

M&MoCS

Shahid Chamran University of Ahvaz

Journal of Applied and Computational Mechanics

Research Paper

Comprehensive Investigating on the Aerodynamic Influences of the Wheel Contact Patch

Xiaoyan Yu[1,2], Qing Jia[1,2], Mohammad Mehdi Rashidi[1,2], Zhigang Yang[1,2,3]

[1] Shanghai Automotive Wind Tunnel Center, Tongji University, Shanghai 201804, China

[2] Shanghai Key Lab of Vehicle Aerodynamics and Vehicle Thermal Management Systems,Shanghai 201804, China

[3] Beijing Aeronautical Science & Technology Research Institute, Beijing, 102211, China

Received June 03 2019; Revised July 18 2019; Accepted for publication August 29 2019.
Corresponding author: Q. Jia (qing.jia@sawtc.com)

Abstract. Computational fluid dynamics is implemented to investigate the influence of the wheel contact patch on the global car aerodynamics. Two main aspects of the problem are the contact step and patch shape. Three important parameters: step height, cut angle, and tire tread shape are taken into consideration. For validations of the numerical results, the experimental data are also considered. The obtained results show that the step height may not significantly affect the global flow field. But when the cut angle increases, the flow separations on the two sides of the front wheel patch will be suppressed successively, which generates two critical points and sudden drag decreases respectively. Besides, tiny differences in tread shape can effectively change the flow rate of the underbody and induce a huge drag discrepancy in the results. In conclusion, the cut angle and tire tread shape must be dealt with carefully in aerodynamic applications of automotive engineering.

Keywords: Vehicle aerodynamics; Wheel contact patch; Tread shape; Contact step; DrivAer.

1. Introduction

Due to the huge demand from the society as well as the government, the requirements for environmentally friendly vehicles has become more urgent now. This promotes all manufacturers to investigate more potential aspects which contribute to energy saving and emission reduction. Vehicle aerodynamics plays an important role in the total drag of automobiles. Therefore nowadays, it has received much attention from all manufacturers and academics. Furthermore, it is reported that the wheels of a passenger car contribute approximately 25% to the total aerodynamic drag [1, 2]. However, wheel aerodynamics is still a foggy field compared with exterior optimization. So in recent years, a large number of industrial and academic investigations have been focusing on wheel aerodynamics [3, 4].

Although several researches have been conducted in wheel aerodynamics, some challenges still remain knotty both in experiments and simulations, one of which is the geometric modeling of the contact patch between wheels and the ground in CFD. The wheel contact patch has been proved to be closely related to the wheel aerodynamics. For example, the contact patch area is the source of the important 'jetting phenomenon' [5], which significantly influences the main flow field. Therefore, it is important to model this patch exactly and deeply understand its effects on vehicle aerodynamics.

However, in CFD, the modeling of the wheel contact patch is not a simple issue. The shape of the contact patch is mainly determined by two aspects. One is the contour of the tire tread, whose impact is proved to be significant on the wheel aerodynamics [6, 7]. The other one is the wheel axis height, which can also change the ground clearance and result in notable flow field differences [8, 9]. Furthermore, when the wheel is rotating, due to the centrifugal force, the paddy rubber tire will be inflated. As a result, the axis will be lifted and the tire tread shape will be altered comparing to the

Published online: October 30 2020

stationary condition [10]. In order to model the tire tread contour and axis height exactly, measurement technology for rotating objects becomes necessary but it is difficult to be realized. Besides, a small step (in this paper, it is named as "contact step") which shares the same shape with the contact patch is commonly added between the wheel and the ground to improve the mesh quality around the contact zone [11, 12]. In numerical simulations, the shape of the patch, as well as the height of the step, is usually defined by engineering experiences. Their influences on vehicle aerodynamics are still unclear and are not taken into consideration so far.

There have been some related former studies published: Millaric [13] tested the different shapes of the contact patch and point out that the patch shape may change the underbody flow around the wheel obviously rather than the main wake of the vehicle, which leads to small drag differences and considerable lift differences. Dianois [11] studied the different contact patch step height on the rotating isolated wheel and concluded that even with tiny changes employed on the step height (0.6 percent of the wheel diameter), huge difference will appear on both the main flow field as well as the aerodynamic forces (about 100 counts on drag coefficients and 200 counts on lift coefficients). These two conclusions reveal that the contact patch may have different influences on a whole car and an isolated wheel. However, the researches on the influence of the contact patch and step differences are still not enough, and more investigations are necessary in this regard. This paper focuses on the aerodynamic influence of the wheel contact patch on a notchback DrivAer. Both aerodynamic forces and flow fields will be evaluated combining with the simulation results. Experimental data are also applied for validations. Finally, several related conclusions and advice will be given for industrial applications.

2. Setups

2.1 Geometry

In this research, the 40%-scaled notchback DrivAer (with mirrors and with smooth underbody) is selected as the car model. The DrivAer model size as can be seen in Fig. 1, is 1.85 m, 0.70 m, 0.57 m in length, width and height, respectively. More information about the DrivAer can be referred to Heft, A. I. et.al [14].

Fig. 1. Notchback DrivAer

In this study, three important parameters are investigated: tire tread shape, axis height, and contact step height. As mentioned above, the first two aspects are related to the contact patch shape and the first one determines the scale of the contact step.

2.1.1 Tire tread shape

Two different wheels are used on the car body, and they are similar to each other in geometry. Both of them equipped the same 5-spoke wheel rim. As the grooved tire can bring notable differences to the global flow field, the slick tire is used in this research. The only difference between them is the contour of the tire tread. Wheel A has a flat tread while wheel B has a slightly convex one, as shown in Fig. 2. Due to this difference, compared with wheel A, the radius of wheel B is bigger by about 0.7% (0.9 mm, from 126.5 mm to 127.4 mm). This discrepancy seems so tiny that it cannot be found without a cautious observation. However, it introduces notable differentiation to the contact patch shape: the patch of wheel A has two straight edges in the front and rear while two arcs take the place of the edges for wheel B (Fig. 3). These two contact patches are in consistent with current studies of Dianois [11] and Millaric [13], respectively.

2.1.2 Axis height

In this study, the wheel axis height is defined by the cut height (H). It means that the patch is obtained by cutting the wheel with a plane that is parallel to the ground and is higher than the bottom of the wheel by H. It is easy to understand that if the cut height increases, the contact patch shape will be changed and its area will increase. In order to eliminate the influence of the wheel radius, the cut angle (θ) parameter is used. The relation between H and θ can be easily derived as (1):

$$\theta = 2 \bullet \arccos(1 - H / r) \tag{1}$$

The detailed description of the cut height, cut angle and contact step can be seen in Fig. 4. On a real sedan, the cut angle is determined by several aspects, such as the total load, wheel rotating speed, tire pressure, and elasticity. Through several measurements, it is concluded that for a common sedan car, the cut angle varies from about 15 to 30°, therefore in this study, the cut angle is set between 14 to 37°.

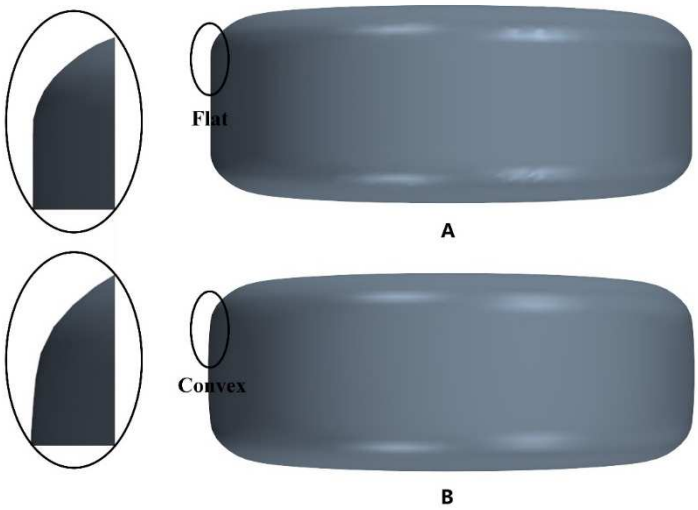

Fig. 2. Wheels with different tires treads

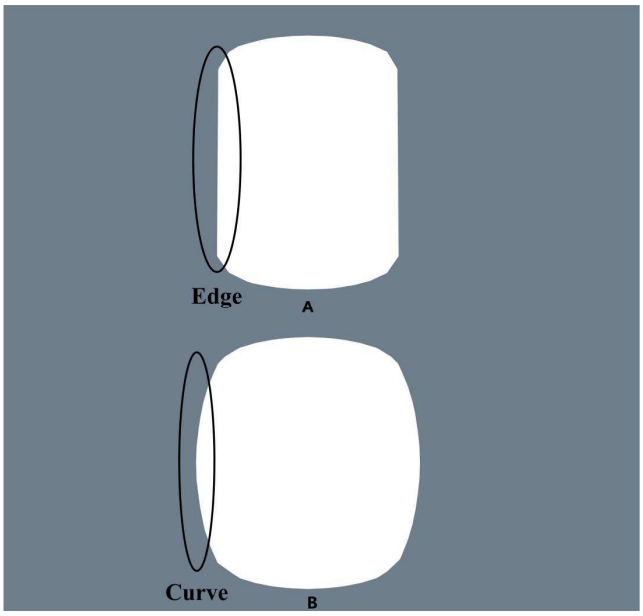

Fig. 3. Wheel contact patches on the ground

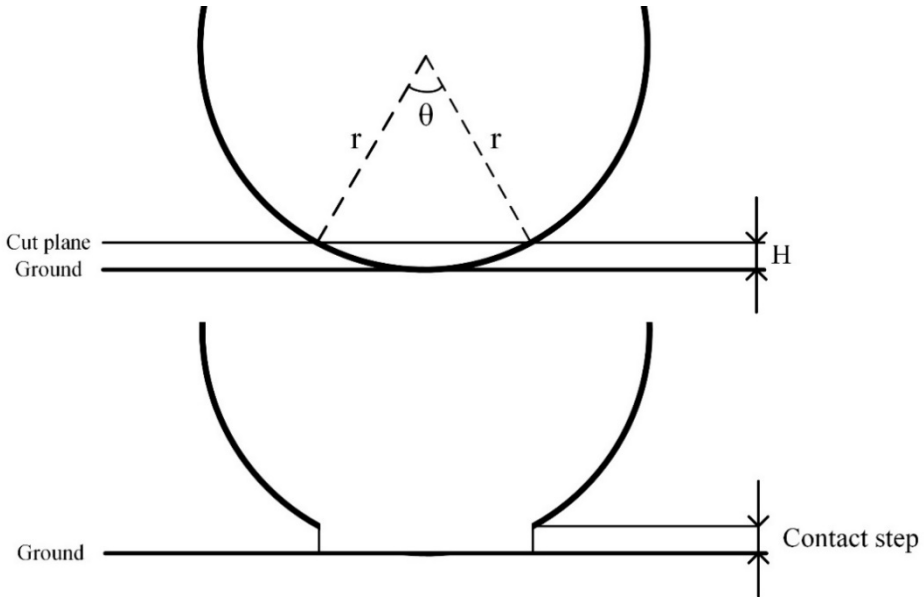

Fig. 4. Cut height (H), cut angle (θ) and contact step.

Table 1. Cases in Group 1

	C1	C2	C3	C4	C5	C6	C7	C8
Cut height(mm)	3.4	3.4	3.4	3.4	3.4	3.4	3.4	3.4
Cut angle(°)	26.5	26.5	26.5	26.5	26.5	26.5	26.5	26.5
Step height(mm)	0.0	0.5	1.0	1.5	2.0	3.0	4.0	5.0

Table 2. Cases in Group 2

	C1	C2	C3	C4	C5	C6	C7	C8	C9
Cut height(mm)	0.9	1.4	1.9	2.4	2.9	3.4	4.4	5.4	6.4
Cut angle(°)	13.6	17.0	19.8	22.3	24.5	26.5	30.2	33.5	36.5
Step height(mm)	0.0	0.0	0.0	0.0	0.0	0.0	0.0	0.0	0.0

Table 3. Cases in Group 3

	C1	C2	C3	C4	C5	C6	C7	C8
Cut height(mm)	1.4	1.9	2.4	2.9	3.4	4.4	5.4	6.4
Cut angle(°)	17.0	19.8	22.3	24.5	26.5	30.2	33.5	36.5
Step height(mm)	0.0	0.5	1.0	1.5	2.0	3.0	4.0	5.0

Furthermore, if the cut angle increases, the body ground clearance will decrease (the relative position between wheels and the car body is the same). As the ground clearance is considered as an important parameter on vehicle aerodynamics, its effect needs to be cleared up so it is also discussed in the following sections.

2.1.3 Step height

By the improvement in simulation technology, the contact patch step can be omitted in some conditions [15] [16] now, which makes the no-step cases possible. However, the step is still necessary when tetrahedron or hexahedron cells are used so it is still necessary to investigate its aerodynamic effects. The step can be seen in Fig. 4. In engineering applications, the height of this tiny step is no more than 10 mm. For the current 40% scaled model, the height is set between 0 and 5 mm correspondingly, slightly greater than its common range. Similar to the cut angle, an increase of the cut height will also increase the body ground clearance, which is necessary to be investigated.

2.2 Cases groups

According to these circumstances, the tested simulations are divided into two basic groups and each group includes 8 different cases:

Group 1: wheel A is used. The cut height remains 3.4 mm in this case (cut angle is 27°) while the step height varies from 0 mm to 5 mm.

Group 2: wheel B is used. The cut height varies from 1.4 to 6.4 mm (cut angle varies from 14 to 37°), the step is omitted.

The detailed setup up of each simulation can be seen in Table 1 and Table 2. It should be mentioned that Case number and Group number are abbreviate to CxGx. For example, Case 1 of Group 1 is abbreviated to C1G1.

Furthermore, the varieties of cut height and cut angle, as mentioned before, can affect the ground clearance, so Group 3 is organized to clarify its influence. In Group 3, wheel B is selected and 8 cases are formed. Each of them has different step heights and cut angles but shares the same ground clearance, as Table 3.

Finally, with further studies, the tire tread shape differences between wheel A and wheel B show a significant impact on total aerodynamics characters, so Group 4 is added for comparisons. C1G1, C6G2, C5G1, and C5G3 are selected in this group, shown in Table 4. C1G1 and C6G2 share the same cut angle and step height but have different tire treads, so as C5G1 and C5G3.

2.3 Computational setup

In this study, Star-CCM+ v12 is used for the numeral simulation due to its ability to generate and compute the no-step cases exactly by the Trimmed Mesh function. The unsteady Reynolds Average Navier-Stokes (URANS) fitted with a realizable k-ε turbulence model is implemented, which has been demonstrated to perform well for flows involving rotation and large-scale separation so it is widely used in the vehicle engineering [17]. The surface mesh size of the main body is set as 4 mm and the size of wheels is set as 2 mm. For the boundary layer, y+ is about 100 so the thickness of the first boundary-layer is set as 1 mm and it can follow the limitation of this turbulence model, the growth rate is set as 1.1 and the total number of layers is set as 5. Non-equilibrium wall function is selected as it is shown to provide a good approximation to the pressure distribution on the surfaces of road wheels [18]. The computational domain is chosen as 11 L (4 L in front of the car model) in length, 8 H in height and 12 W in width to avoid the interference from the boundaries [19] and the blockage ratio is limited to 1%.

Table 4. Cases in Group 4

	C1G1	C6G2	C5G1	C5G3
Wheel	A	B	A	B
Cut angle(°)	26.5	26.5	26.5	26.5
Step height(mm)	0.0	0.0	2.0	2.0

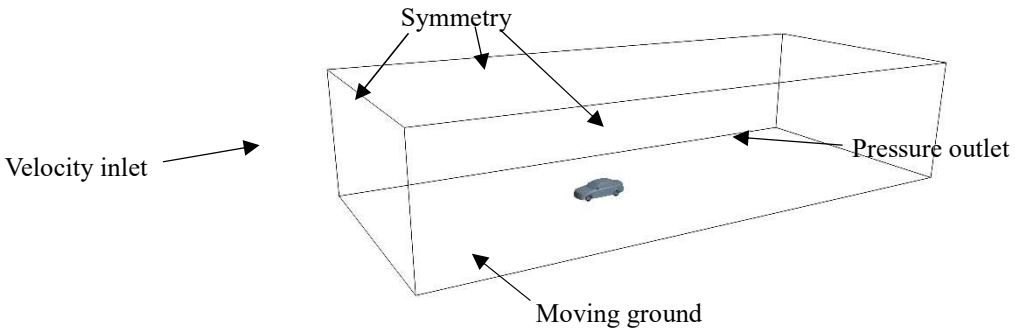

Fig. 5. Cut height (H), Cut angle (θ) and contact step

Table 5. C_D and C_L of different meshes

	Number of Elements	C_D	C_L
Baseline	17 million	-	-
Refined-1	19 million	+0.001	-0.002
Refined-2	21 million	0	-0.001

2.4 Boundary conditions

The inlet velocity is set at 40 m/s with a turbulence intensity of 1%. In this situation, the Reynolds number based on the wheel diameter is 1.26×10^6, meeting the Reynolds number independence requirement proposed by former papers [14], [20]. The angular velocity of wheels is about 314 rad/s, which ensures the linear velocity of wheels at the tire tread is equal to the freestream velocity. At the outlet boundary, a pressure-outlet boundary condition specified with a gauge pressure of 0 is used. A symmetry boundary condition was specified on the walls to avoid the interference of the boundary-layer from these surfaces. The wheel rotation method is set as following: Sliding Mesh method is selected on wheel rims and rotating wall is selected on the tire. The accuracy of this method has been proved in former studies [20]. The wheel rim rotates 1° in each time step and the total calculation time is equal to 10 rotation periods. The computational domain and boundary conditions can be seen in Fig. 5.

2.5 Grid independence

In order to eliminate the interference of grid dependency, a grid study is conducted. C1G1 is selected and 3 different meshes are generated by shrinking the maximum volume of grids. Drag and lift coefficient varieties are used for grid study. The number of elements and the obtained results are presented in Table 5.

It can be concluded that although the total mesh becomes denser, C_D and C_L both have no noteworthy changes. Therefore, the baseline mesh is applied for both models in this study, while the total number of cells is about 17 million. More related information about this study can be found in [20].

2.6 Numerical validation

2.6.1 Aerodynamic coefficients

Numerical validation is of great significance for a CFD simulation. In this study, both aerodynamic coefficients and the local flow field are concerned. In Table 6, the drag coefficients of experimental data cited from several presented papers are given while the delta between C1G1 and experiments (sim. minuses exp.) are listed. All the experiments share the same car and wheel configurations with the current study except the model scale.

It is demonstrated that although different experimental data vary as much as 30 counts (more than 10%), the differences between the simulation result of C1G1 and those experiments are mainly about 6% or lower. The discrepancy between the presented simulation and experiments may not be explained penetratingly. But in general, as all the drag coefficients contained in the following sections do not have great changes, these differences are not notable.

2.6.2 Local flow field

The flow field investigation is conducted by the surface pressure coefficients (C_P) comparisons. The pressure distribution on the centerline of the car body is shown in Fig.6. Experimental data from Peichl [16] and Heft [14] are included. As the wheel region has no notable effect on the upper body, only the underbody pressure is posed. It can be seen that in most parts (middle and rear regions), the differences between experimental data and numerical simulation are relatively small. Besides, pressure distribution on the z=60 mm plane of the body is also concerned. In Fig.7, it can be seen that the experimental and simulation data have a good agreement, which indicates that the local flow field near the side and the rear end of the car body are simulated accurately in this study.

In conclusion, concerning the different equipment in these configurations, the accuracy of the CFD simulation is acceptable so the CFD results in this paper are considered trustworthy.

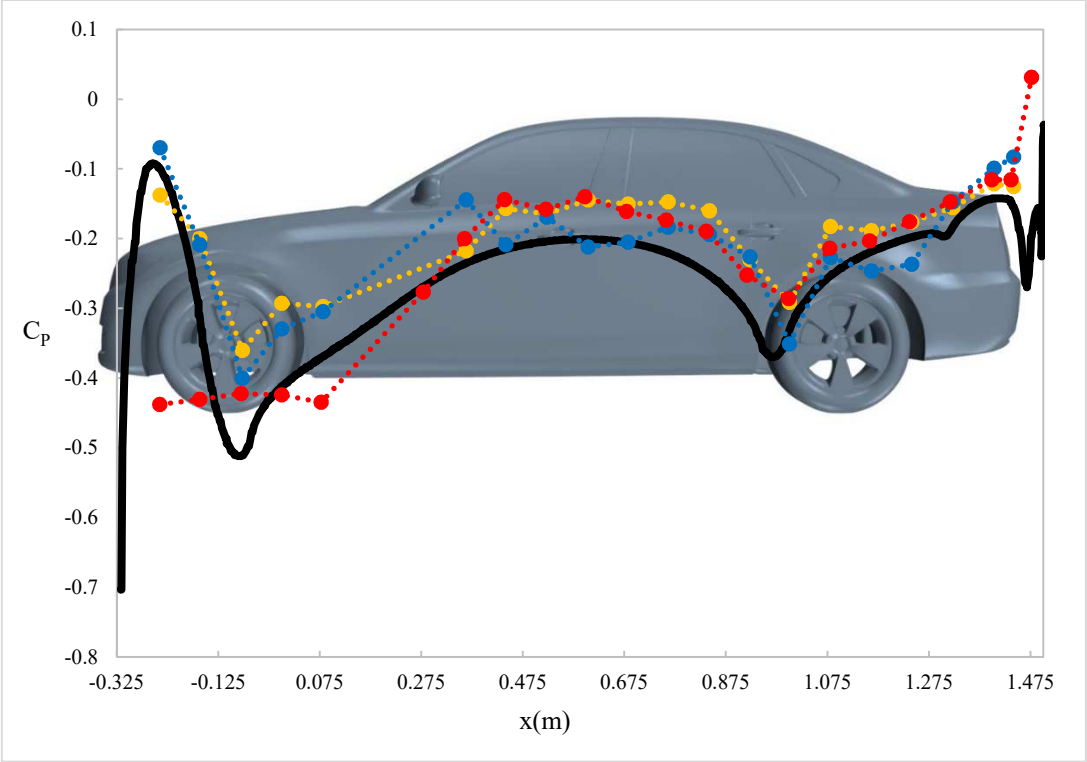

Fig. 6. C_P on the centerline of the underbody (Black: CFD of C1G1; Red: Notchback exp. in TUM WT [16]; Blue: Notchback exp. in AUDI WT [16]; Yellow: Fastback exp. in TUM WT [14])

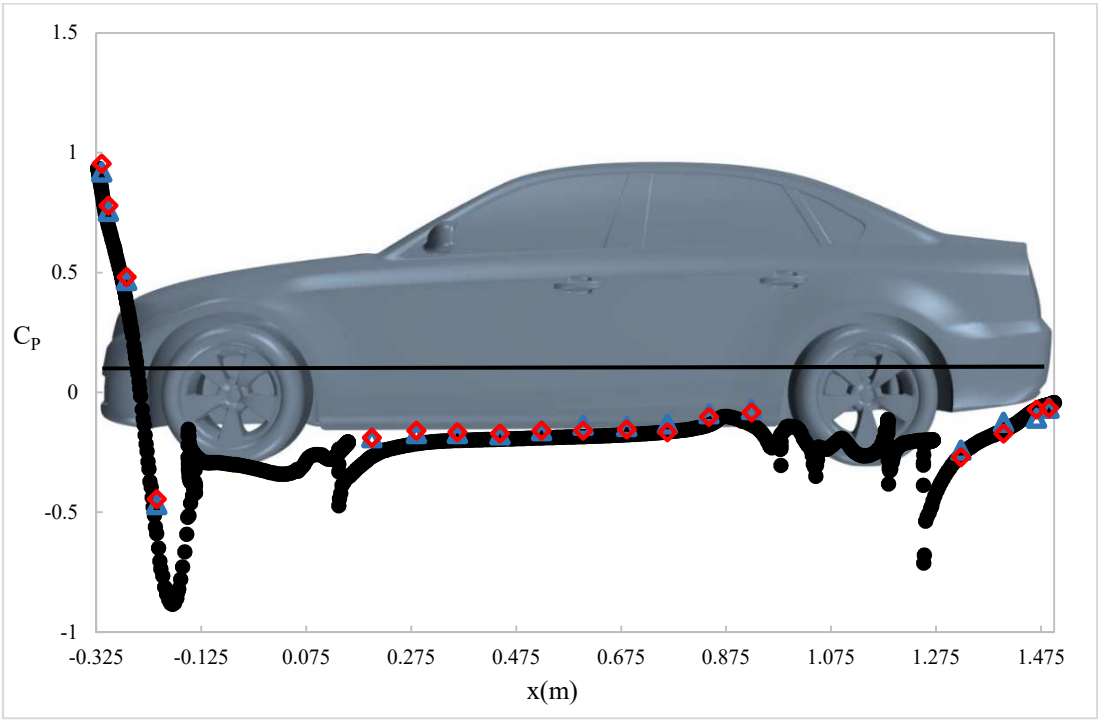

Fig. 7. C_P on z=60 mm plane of the body (Black: CFD of C1G1; Red: Notchback exp. in TUM WT [16]; Blue: Notchback exp. in AUDI WT [16])

3. Results and Discussion

In this section, the simulation results of the 4 groups will be presented. Most of the obtained results in this study are time-averaged in the last 5 rotation periods.

3.1 Group 1: step height

The drag coefficient of Group 1 can be seen in Fig. 8.

Table 6. C_D comparisons with experiments

	C_D	ΔC_D	Percentage
C1G1	0.239	-	-
TUM, exp, 2012. [14]	0.246	-0.007	-2.85%
Audi, exp, 2014. [21]	0.254	-0.015	-5.91%
TUM, exp, 2016. [21]	0.255	-0.016	-6.27%
PVT, exp, 2015. [22]	0.231	+0.008	+3.46%
Audi, exp, 2016. [23]	0.255	-0.016	-6.27%
FKFS, exp, 2018. [24]	0.261	-0.022	-8.43%

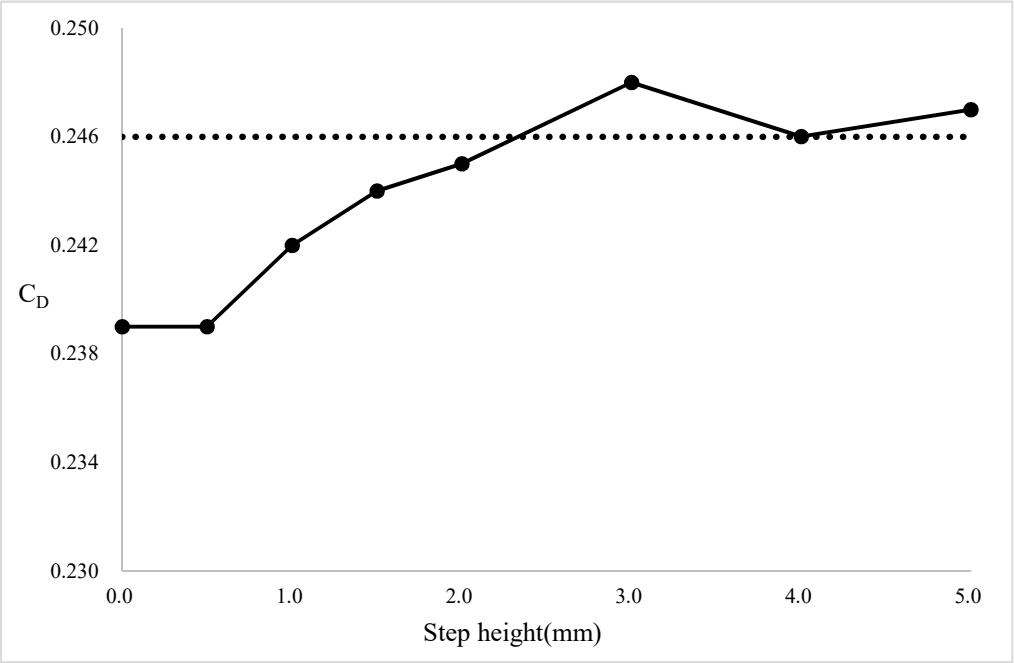

Fig. 8. C_D in Group 1 (the dotted line represents exp. in [14]).

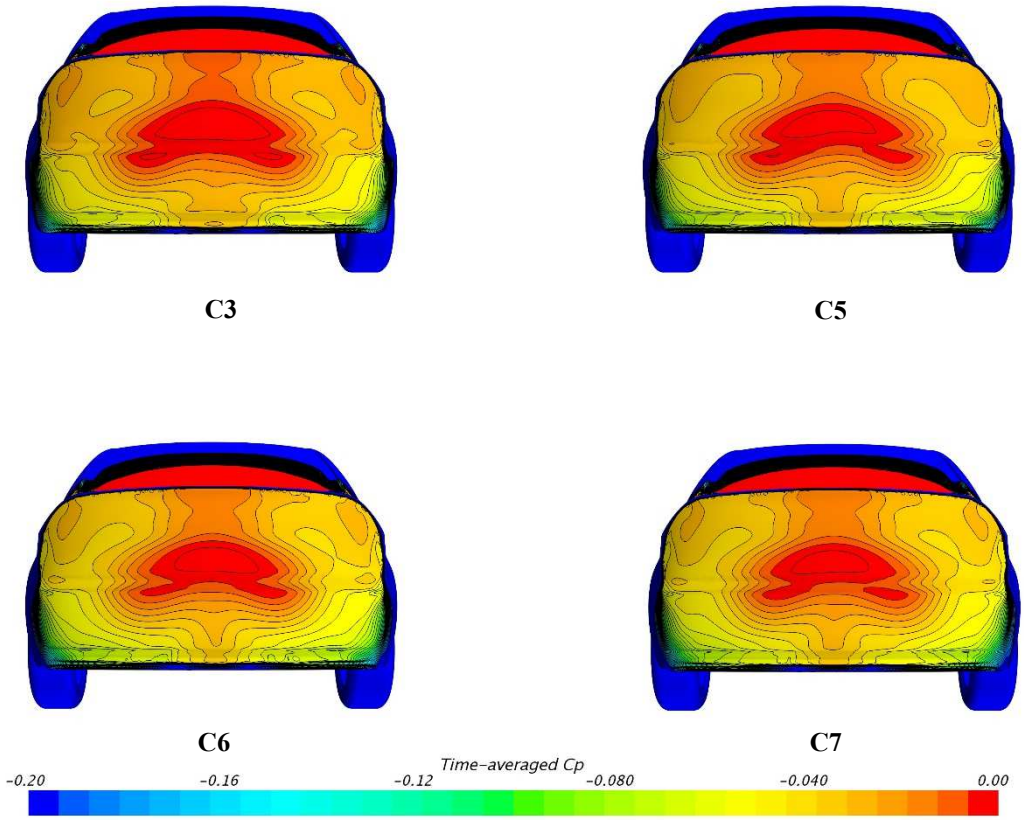

Fig. 9. C_P on the base.

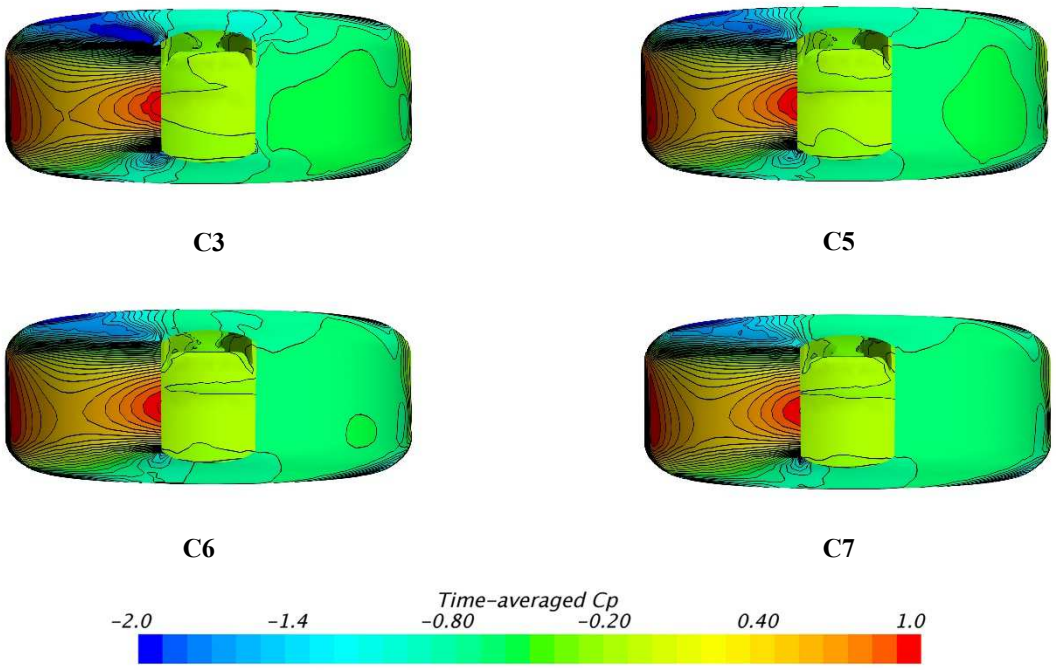

Fig. 10. C_P on the front-left wheel.

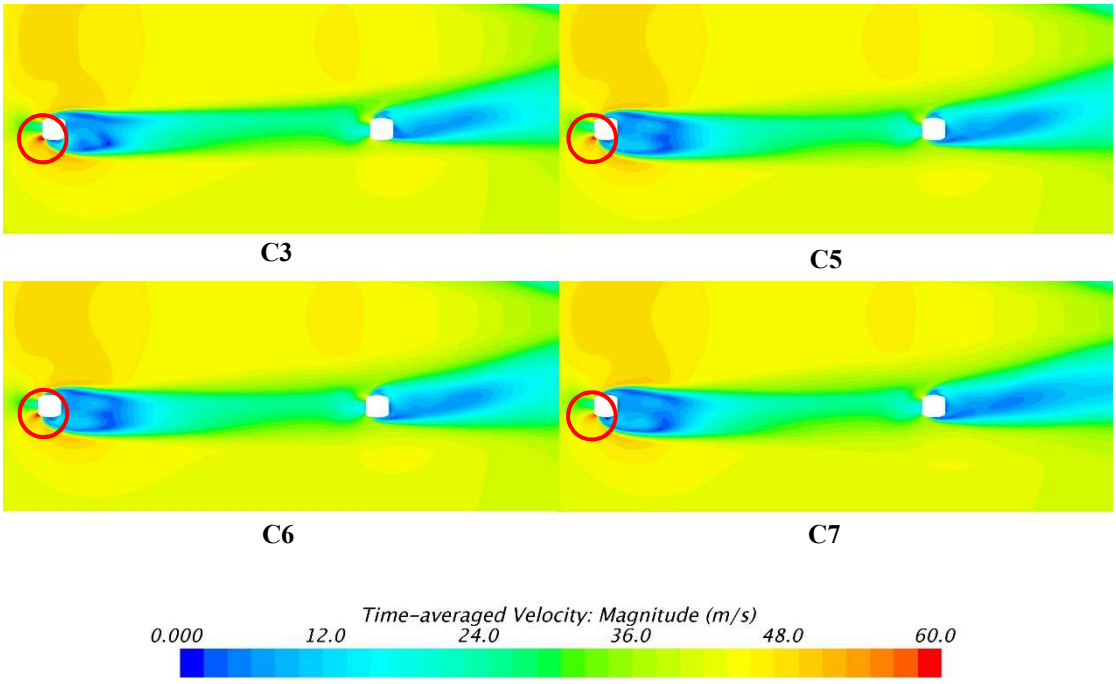

Fig. 11. Time-averaged velocity on z=-0.12 m.

In this figure, it can be concluded that while the step height increases (from 0 to 5.0 mm), the total aerodynamic drag experiences a slight increase as well (about 8-10 counts) though a small oscillation appears. In order to study the source of the drag increment and understand the aerodynamic influence deeply, it is necessary to analyze the flow field characteristics. In order to simplify flow field characteristics comparisons, only 4 cases (C3, C5, C6, and C7) are included. In Fig. 9, the static pressure coefficient (C_P) distribution on the car base can be seen. Corresponding to the body aerodynamic drag, although the base pressure is slightly reduced, which leads to the higher drag of the car body, its differences are not too remarkable and may not bring great changes to the total drag. This phenomenon reveals that the step height may not affect the main wake significantly.

However, notable varieties have emerged on the local flow field of the wheels. Fig. 10 shows the C_P distribution on the contact patch region of the front-left wheels. It can be seen that the pressure on the outer side of the wheel increase greatly. Besides, the pressure on the rear part of the wheel experiences a slight decrease and this may explain the increase of wheel drag. Combining the fluid dynamic theory, it is conjectured that the pressure increase on the wheel side results from the heightened clearance between the bottom of the wheel and the ground, which is named as "wheel clearance" in this paper.

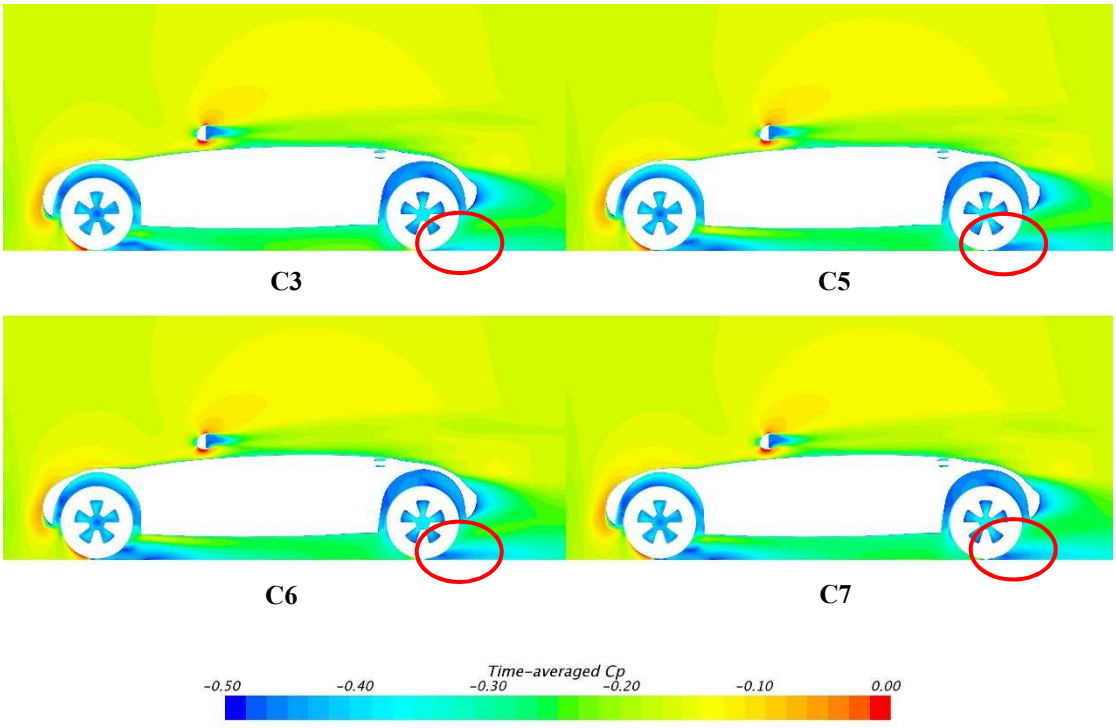

Fig. 12. Time-averaged velocity on y=0.338 m.

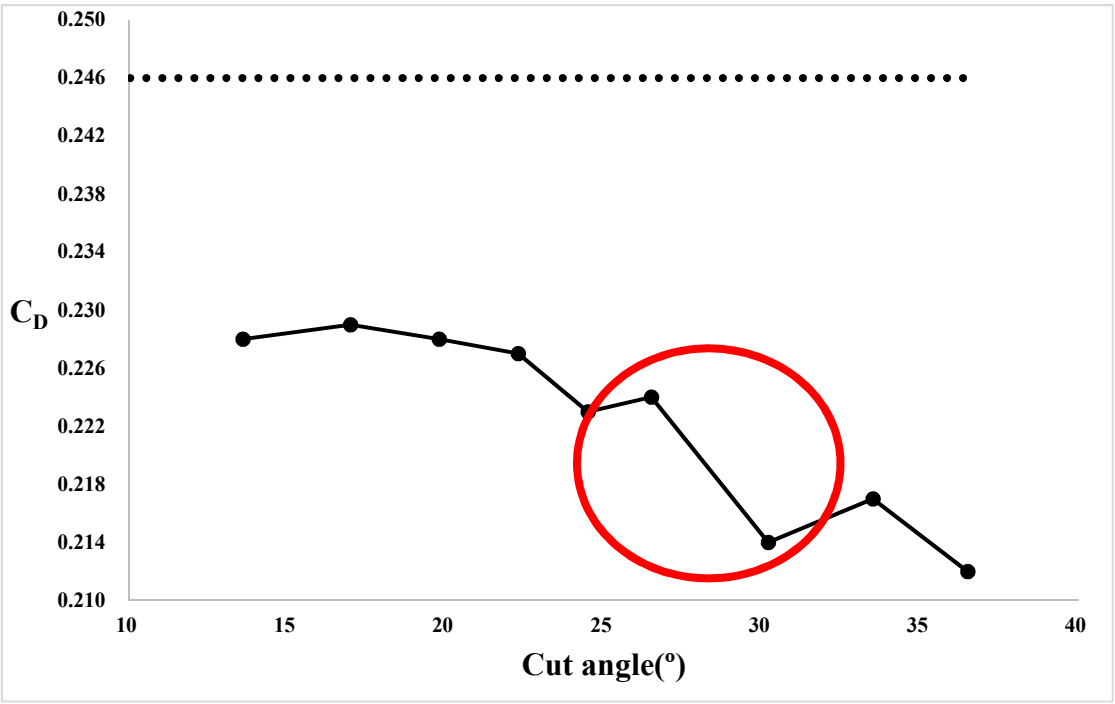

Fig. 13. C_D in Group 2.

As the step is heightened, the wheel clearance increases as well and slows down the flow around the contact patch. At the same time, the higher step produces larger separation behind the patch, which leads to lower wheelbase pressure and higher wheel drag. This effect is similar to the classic cylinder flow vortexes. Due to these circumstances, the local flow field around the wheel obviously may be influenced by the contact step and some further comparisons are required.

Fig. 11 illustrates the time-averaged velocity near the wheel patch region (plane z=-0.12 m, about 5 mm higher than the ground). The reduced flow velocity on both sides of the wheel patch can also be found (marked in red oval). Besides, wake direction and structure of the front wheel is slightly altered, which affects the rear wheel and the wake of the vehicle. But in general, although the pressure on the bottom of the wheel increases notably, the differences in the local flow field are still relatively small.

Similar conclusions can be drawn by comparing the global flow field. In Fig. 12, time-averaged velocity magnitude on the longitudinal plane y=0.338 m can be seen, which crosses the center part of the left wheels. Even though the wheel wake is changed notably (marked in red), the global velocity and main body wake still seem no notable differences.

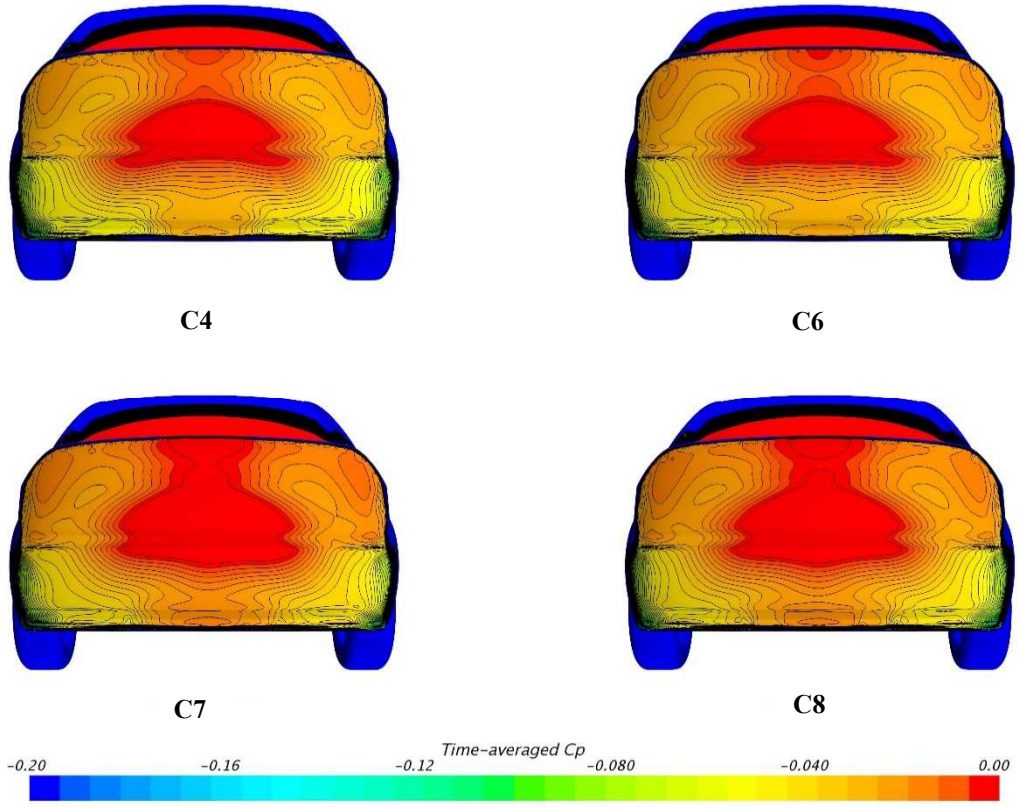

Fig. 14. C_P on the base.

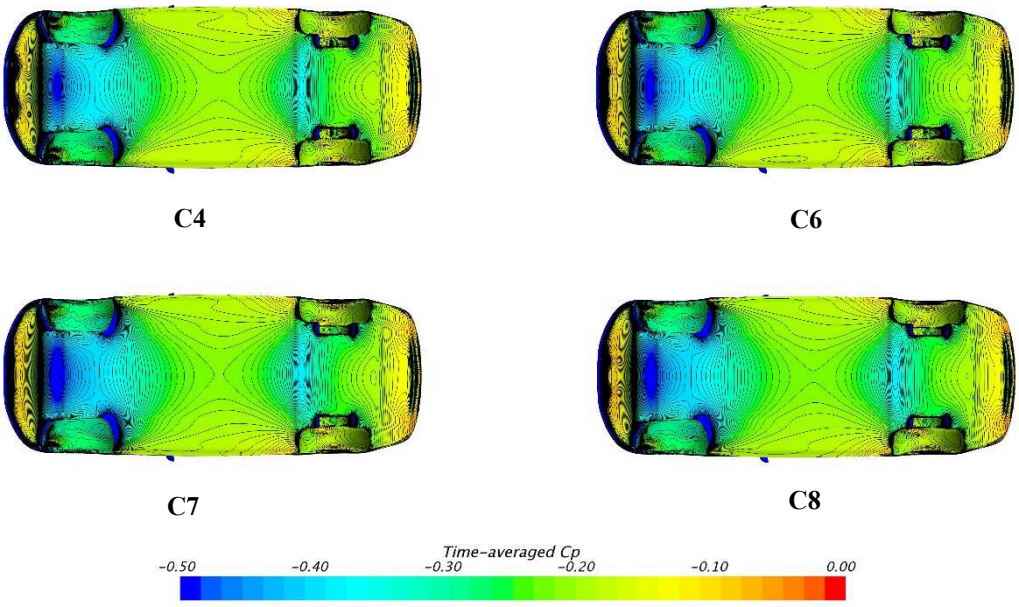

Fig. 15. C_P on the underbody.

In summary, as the step height increases, the wheel clearance increases, too. The flow slows down in the contact patch region and the pressure gets higher significantly. Increased height induces the larger separation behind the front step, so the wheel wake is strengthened and local pressure reduces. The strong wheel wake may also enhance the body wake, which can lead to the drag increase on both wheels and the car body. But in general, the overall influence of the step height on the total drag and flow field is still not of great significance. For a common drag-study problem, the existence of the contact step may not affect the total result to some degree. So adding a suitable step for higher mesh quality is feasible.

3.2 Group 2: cut angle

The drag coefficient of Group 2 can be seen in Fig. 13. It is demonstrated that the total drag keeps at about 0.225 while $\theta \leq 26.5^{\circ}$. However, when the cut angle reaches 30º, a sudden decrease (about 10 counts) is arisen. Furthermore, another

small decrease (about 5 counts) is also observed when the angle reaches about 35º. Compared to Group 1 and experiments, the drag coefficients in Group 2 is 10-15% (about 20-30 counts) smaller. These differences, which may result from the tire tread shape, are considerably great and need further investigations.

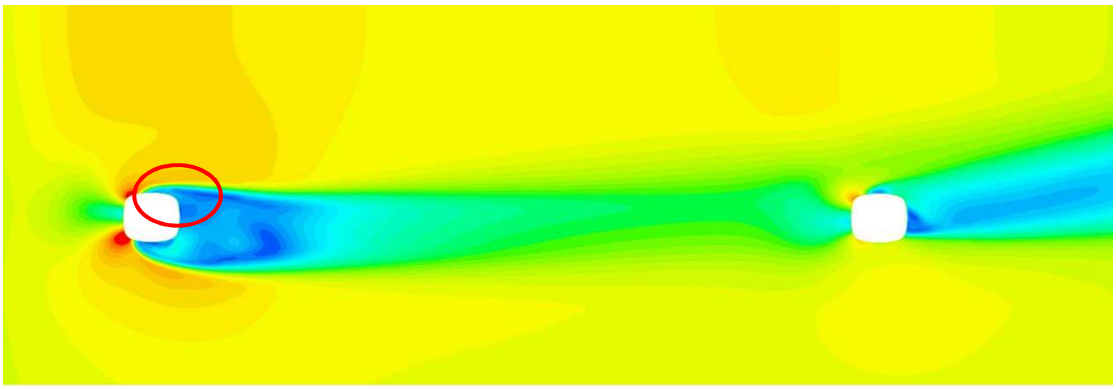

C6

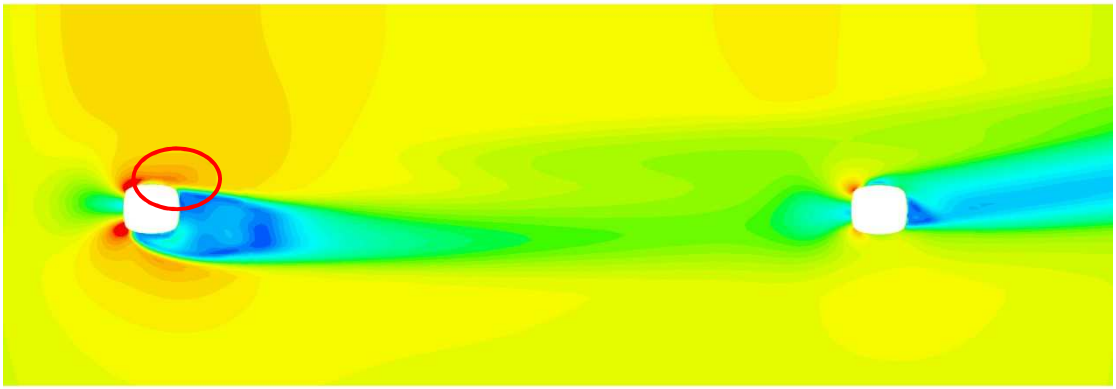

C7

Fig. 16. Time-averaged velocity on z=-0.12 m.

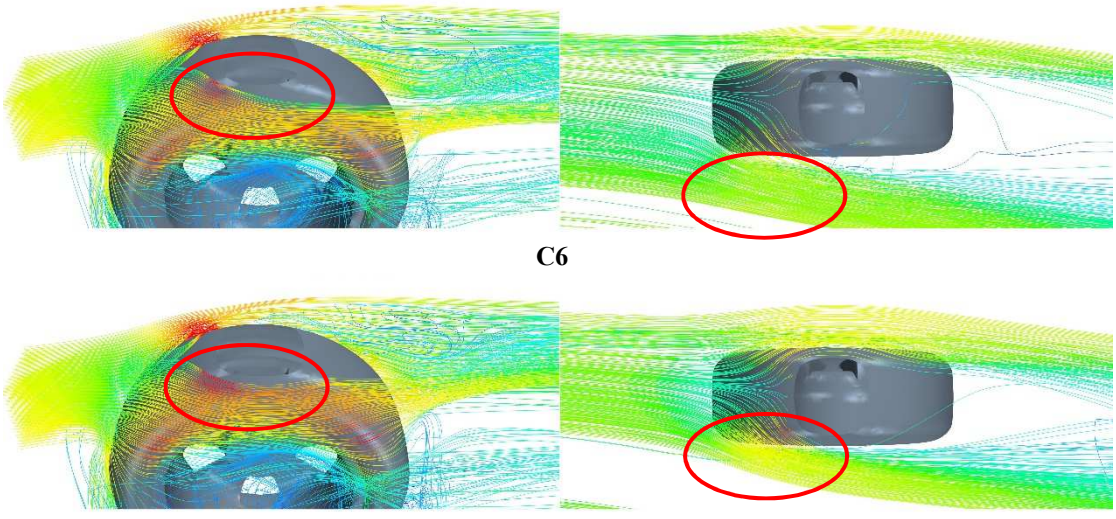

C6

C7

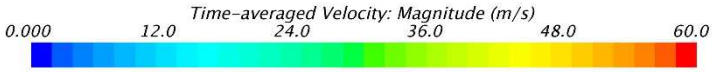

Fig. 17. Streamlines near the wheel patches (left: front; right: rear).

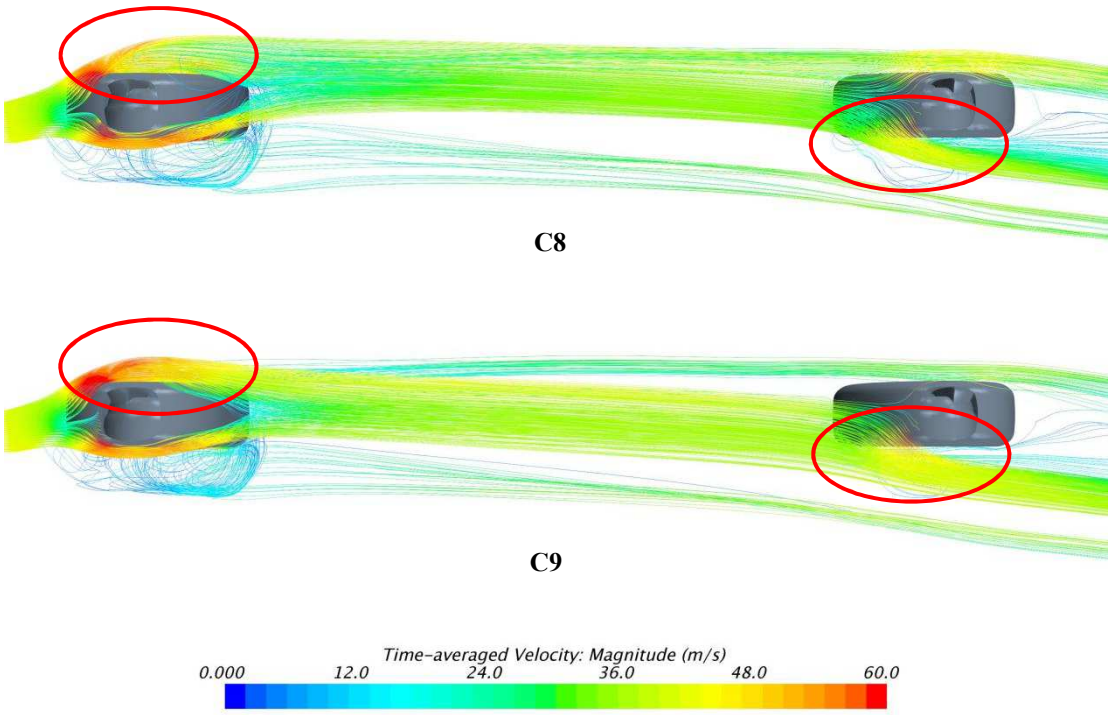

Fig. 18. Streamlines near the wheel patches.

As the decrease appears between C6 and C7, only C4, C6, C7, and C8 are chosen for flow field studies (cut angles are 17.0º, 22.3º, 26.5º, 30.2º and 33.5º). The pressure coefficient on the car base and underbody can be seen in Fig. 14 and Fig. 15. For C5 & C6 and C7 & C8, both the base and underbody pressure are similar. However, when C6 and C7 are selected for comparisons, the clear increment can be observed on the car base, which explains the drag reduction well. Besides, differences in underbody pressure are more obvious than the base. So this reveals that the underbody flow is altered greatly rather than the upper-body flow due to the larger cut angle.

Therefore, the flow field difference between C6 and C7 should be concerned carefully. Fig. 16 shows the velocity near the left wheel patch region of C6 & C7. In Fig. 16, one important flow characteristic can be observed: on the inner side of the front wheel patch, the flow separation in C6 is suppressed in C7, marked in the red oval. Due to this suppression, the flow around the inner side speeds up, which weakens the wake of the front wheel certainly and alters its direction outwards. So it can be assumed that the weakened wheel wake may reduce the strength of the vorticity of underbody flow. As a result, the body wake which related to the underbody flow is also weakened, which finally results in lower total drag.

This phenomenon can be seen clearer in streamlines. In Fig. 17, it is concluded that the separation suppression results from the geometry changes of the wheel patch. As the cut angle increases, the shape of the patch size is altered, too. Due to this situation, the adverse pressure gradient is not great enough so the flow separation disappears.

Besides, when comparing the streamlines of C8 (33.5º) and C9 (36.5º), the flow changes around the outer side of the front wheel patch are also notable, seen in Fig. 18. It is illustrated that the outer side flow tends to be deflected insides and most of the rear wheel flow is turned insides. This can explain the small decrease when the cut angle reaches 35º. Furthermore, it can be assumed that if the cut angle continues to get larger, the separation on the outer side of the front patch may also been suppressed, which means another potential critical point exists and this may bring more influence on the whole flow field.

The influence of the cut angle can be concluded as following: cut angle may not affect the flow field when it is not large enough. However, when the angle reaches a critical value (named "critical point" in this paper, which is located within the range of 26.5º to 30.2º in Group 2), a sudden decrease will arise. This decrease results from the local flow field near the front contact patch. At this critical point, the separation on the inner side of the patch will be suppressed. This suppression will reduce the wheel wake and change its direction. Finally, the higher speed of inner side flow is reached and the drag is reduced significantly. Following the increased cut height, the outer side flow field of the front patch may also be suppressed, which leads to further impact on the total aerodynamic coefficients. Due to its influence on both total drag and local flow field, the cut angle should be considered as an important parameter in engineering design and its effect of aerodynamics coefficients should be carefully investigated.

3.3 Group 3: ground clearance

Drag results of Group 3 are shown in Fig. 19. The results of Group 2 are also included in red color for comparison.

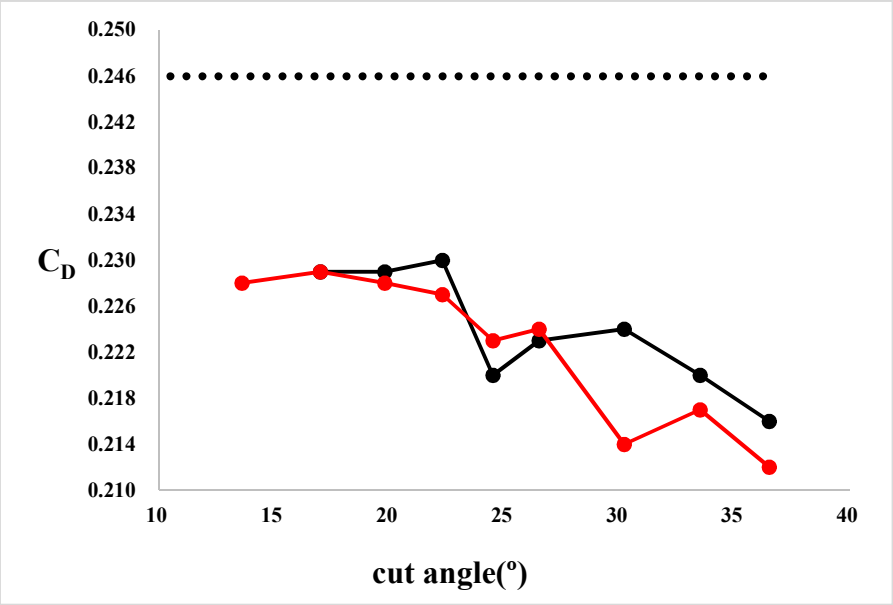

Fig. 19. C_D in Group 3 (red line represents C_D in Group 2).

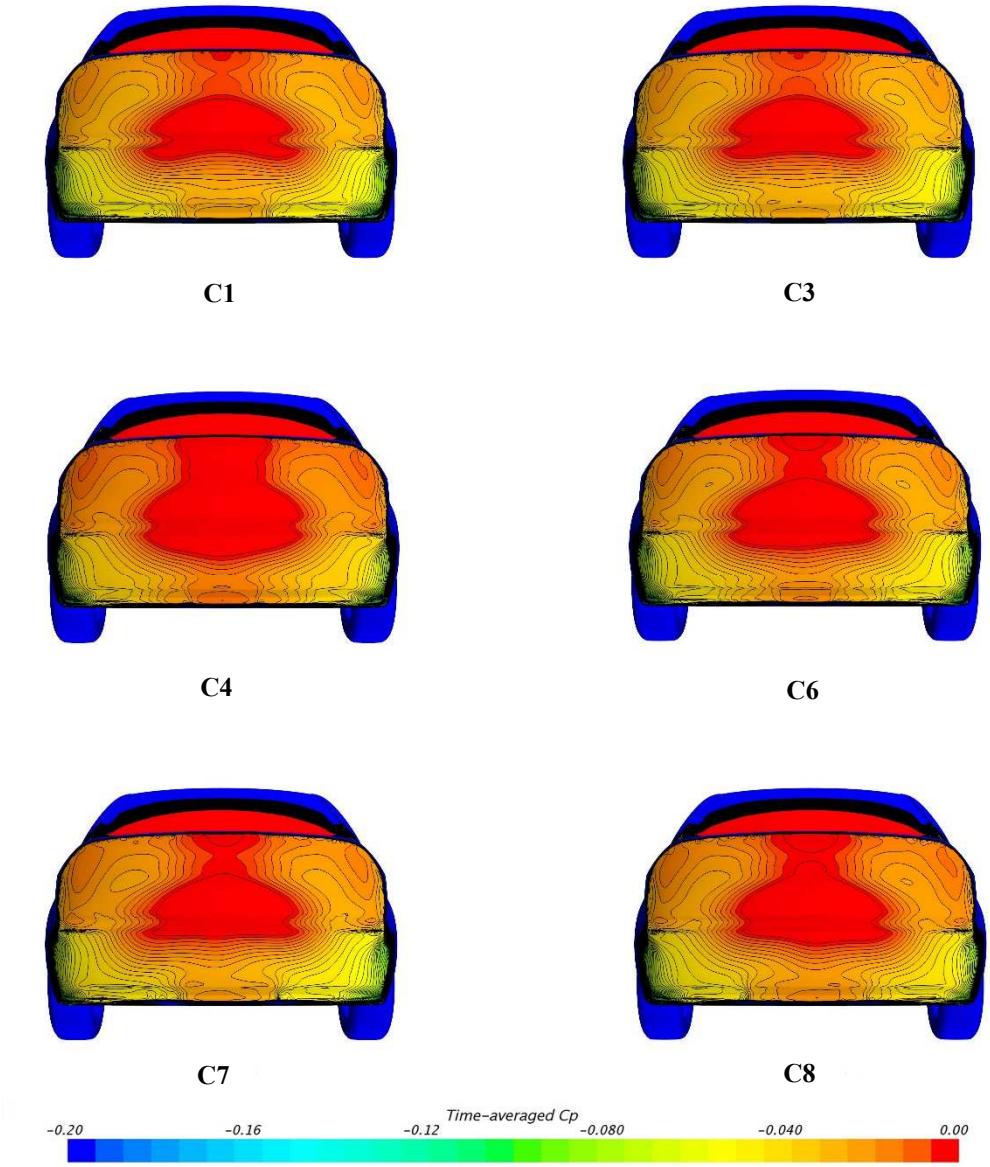

Fig. 20. C_P on the base.

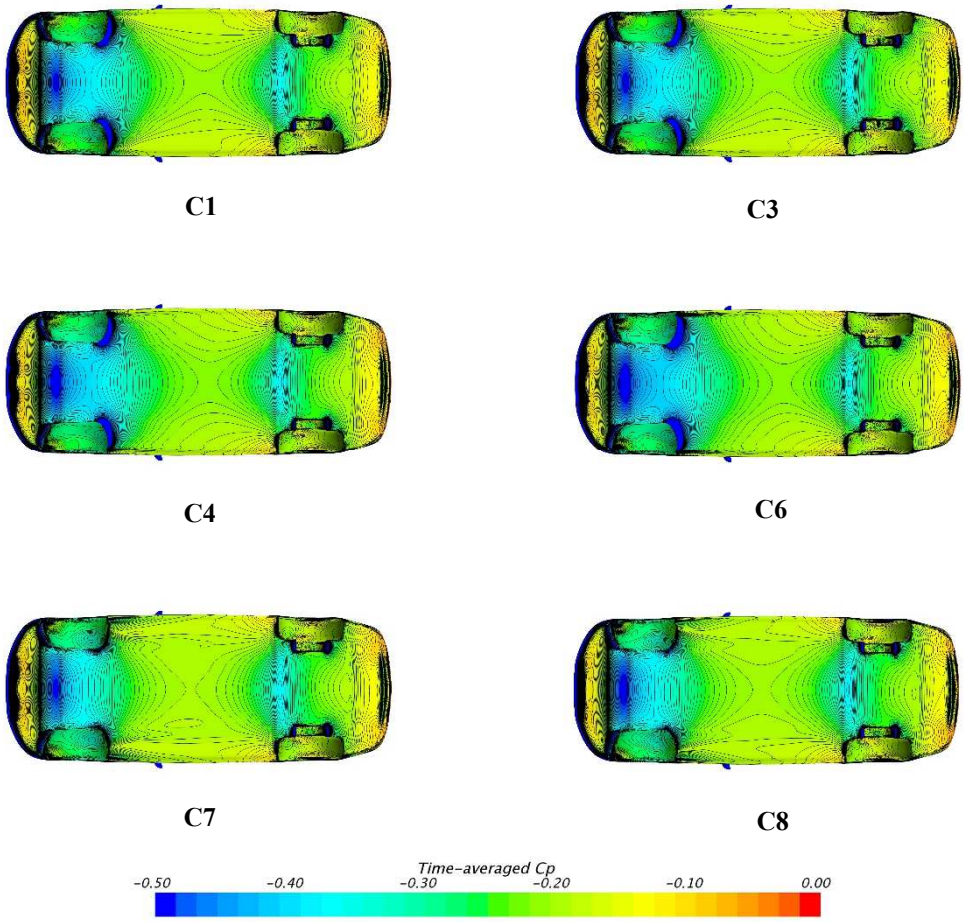

Fig. 21. C_P on the underbody.

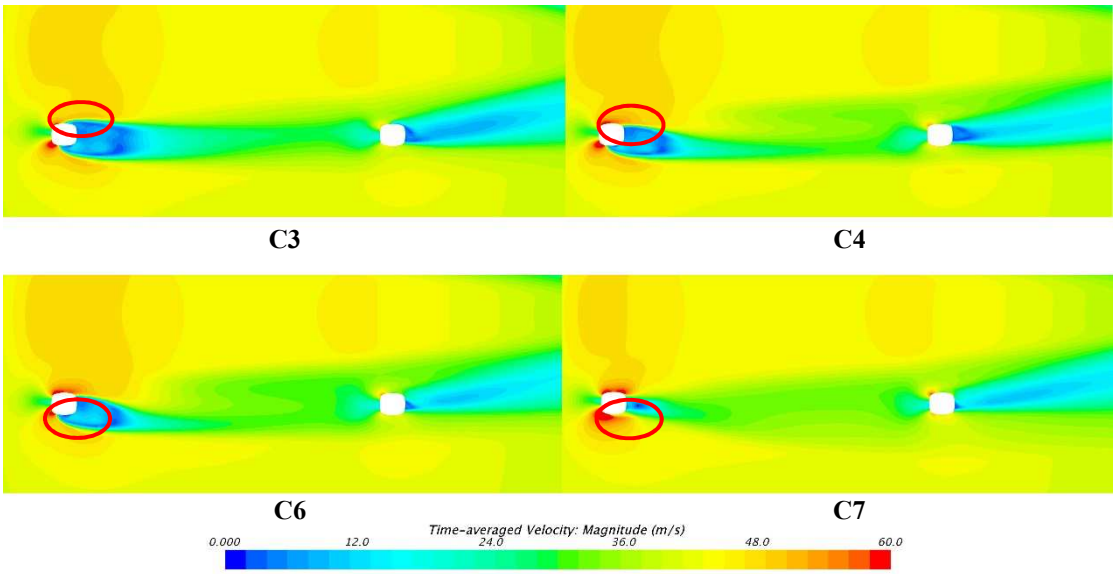

Fig. 22. Time-averaged velocity near left wheel patches on z=-0.12 m.

In Group 3, although the step height increases together with the cut angle, its overall trend is similar to which in Group 2. As the cut angle and step height increases, the total drag coefficient decreases by about 15 counts. Besides, the overall drag value is also consistent with Group 2, which has a notable discrepancy compared with Group 1 and experimental data. The large drag decrease (about 10 counts) can also be observed. However, different from Group 2, the position of the critical point is altered, from 22.3-24.5º in Group 3. Besides, when the cut angle reaches about 35º, the reduction of C_D shown in Group 2 still exists. It seems that even though the contact step is built and the ground clearance is fixed, the main effect of the contact patch shape is not changed greatly. Furthermore, the effect of the wheel drag increase derived from the contact step in Group 1 is not obvious, either.

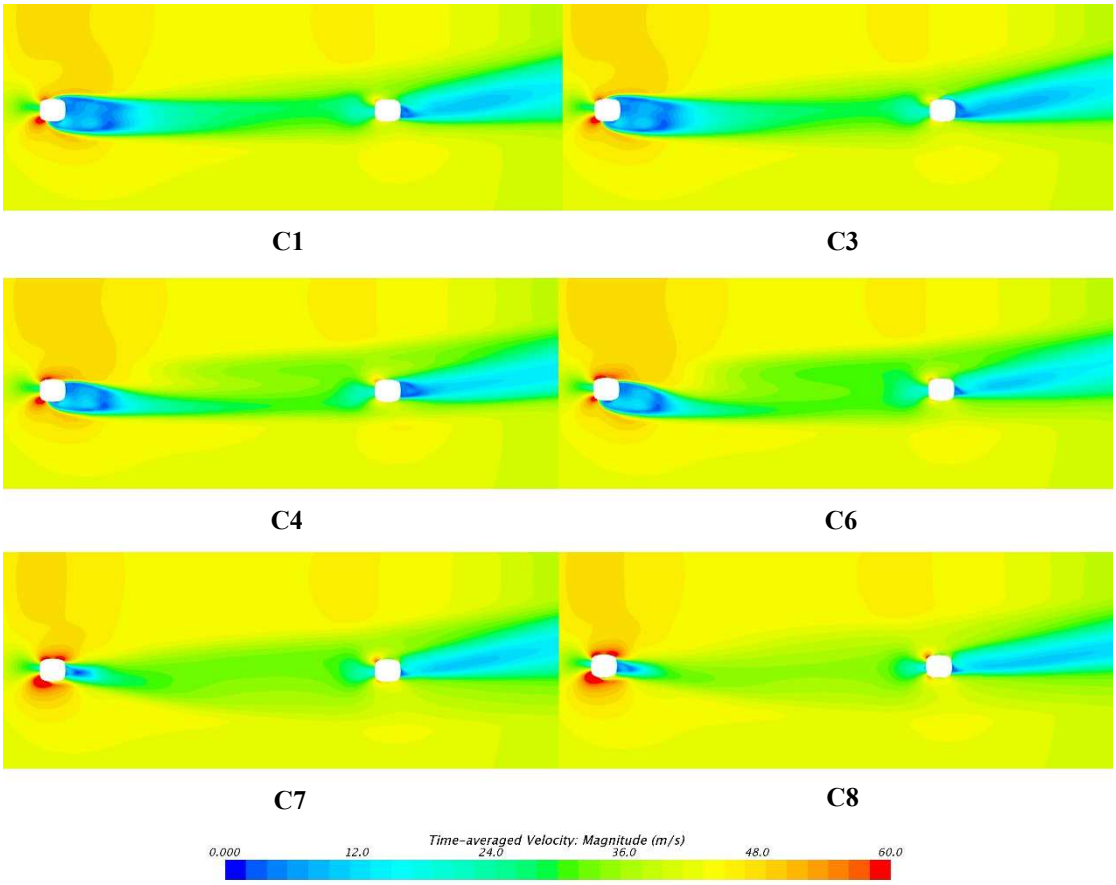

Fig. 23. Time-averaged velocity on z=-0.12 m.

Due to the more complex drag changes, it is necessary to choose more cases for flow field comparisons in this group: C1, C3, C4, C6, C7, and C8 (cut angles are 22.3º, 26.5º, 30.2º and 33.5º). Fig. 20 shows the base pressure of them. The differences of C_P are consistent with the drag changes between cases, which reveal that the main drag contribution is still attributed to the base region. However, as the drag oscillation is more obvious than Group 2, it is difficult to figure out a single trend in Group 3. In order to explain the effect in this group, some more analyses need to be conducted.

Fig. 21 illustrates the underbody C_P of 6 cases. It can be seen that unlike the drag and base pressure, underbody pressure shows more regularities and these 6 cases can be divided into 3 pairs. Pair 1 includes C1 (cut angle is 17.0º) and C3 (22.3º). Pair 2 includes C4 and C6 (24.5º and 30.2º) while Pair 3 includes C7 and C8 (33.5º and 36.5º). In each pair, the underbody pressure distribution is similar but obvious discrepancies lie between pairs.

The source of these flow field differences between pairs can be seen in Fig. 22, which demonstrates the time-averaged velocity near the wheel patches. Between Pair 1 and Pair 2, the critical point which is shown in Group 2 can be found again. When the first critical point is reached, the separation on the inner side of the wheel patch is suppressed due to the changed patch shape. This critical point seems to have the same effect as which in Group 2 although its specific cut angle becomes smaller (from about 30º to 25º). Furthermore, between Pair 2 and Pair 3, another critical point is reached and the separation on the outer side of the wheel patch also disappears, which weakens the front-wheel wake and greatly changes the underbody flow field. As mentioned above, although this critical point is not observed in Group 2, its evidence can still be found between C7 and C8. These phenomena imply that the critical point in Group 2 still exists in the total flow field of Group 3. However, the number and specific positions are both changed. In other words, the existence of the contact step may not alter the global influence of the contact patch on the flow field, but it can obviously change the position of the important critical points.

Furthermore, as shown in Fig. 20, it is demonstrated that even in the same pair, the local flow field is not completely the same. Fig. 23 shows the time-averaged velocity of the left wheel patch near the ground for 3 pairs. In Pair 1, while the cut angle increases, the direction of the front wheel wake is slightly altered, which also changes the strength of the rear patch separation. In Pair 2, this phenomenon can be observed more clearly. In Pair 3, the flow velocity around the front patch continues to be accelerated, which weakens the front-wheel wake and enhances the underbody flow near the rear patch, which results in further drag reduction. This reveals that the flow features become more complex because of the existence of the contact step. Tiny changes on the front wake may notably influence the rear part flow field of the car.

In summary, according to the underbody flow field, cases in Group 3 can be divided into 3 pairs while the cut angle and step height increase together. Between each pair, a critical point can be found. When these points are reached, the flow separation on the inner and outer side of the front wheel patch is suppressed respectively and the front wheel wake is weakened as well as the body wake. This phenomenon is consistent with the effect of the cut angle increase in Group 2,

even though the position of the point and the strength of the effect is changed. Besides, the effect of cut height and wheel clearance increase in Group 1 cannot be observed here, so it can be surmised that the influence of the patch shape is greater than the two in the preamble. However, the position of the two critical points gets smaller and is easier to be reached in engineering applications when the step exists. The flow field also gets more complex and sensitive due to the step so the effect of the step height still cannot be ignored.

3.4 Group 4: tire tread shape

The results of Group 4 is shown in Table 7.

Table 7. Cases in Group 4

	C1G1	C6G2	C5G1	C5G3
Wheel	A	B	A	B
Cut angle(°)	26.5	26.5	26.5	26.5
Step height(mm)	0.0	0.0	2.0	2.0
C_D	0.239	0.224	0.245	0.223

Comparing C1G1 and C6G2, it can be seen that while the contact step is omitted, the total drag coefficient of the car will reduce 15 counts (about 6.2%) if wheel B (curve edge) takes the place of wheel A (sharp edge). Besides, comparing C5G1 and C5G3, when a small contact step (2mm in height) is added, this drag reduction effect will increase greatly, up to 22 counts (about 9.0%). For a general sedan, this effect is considerable and needs studying deeply. As the radius differences between these two wheels are only 0.9 mm (about 0.7%), it is highly possible that this reduction effect may result from the tire tread shape.

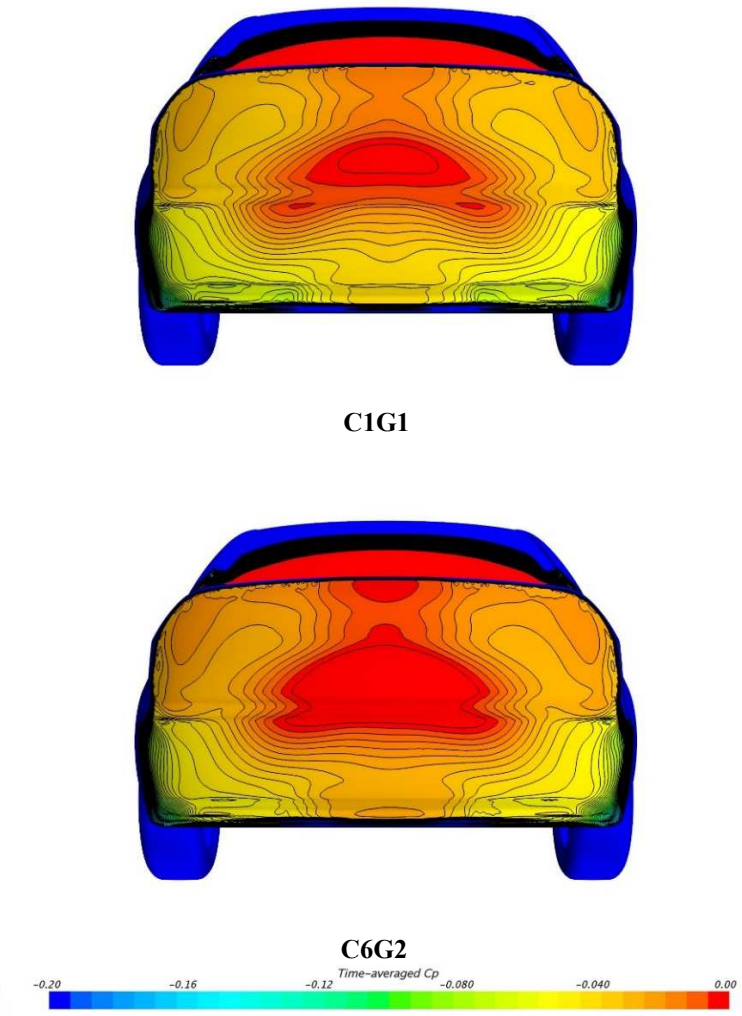

Fig. 24. Base C_P of Pair 1.

For convenient further comparisons, the four cases are divided into two pairs: Pair 1 contains C1G1 and C6G2 while Pair 2 contains the other two. These two pairs will be investigated respectively. Fig.24 shows C_P on the car base of Pair 1. It can be seen that the base C_P of C6G2 increases notably. Besides, the increment is distributed in most regions of the base, especially in the central part. So the drag reduction may be still closely related to the weakened body wake, which is derived from the underbody flow.

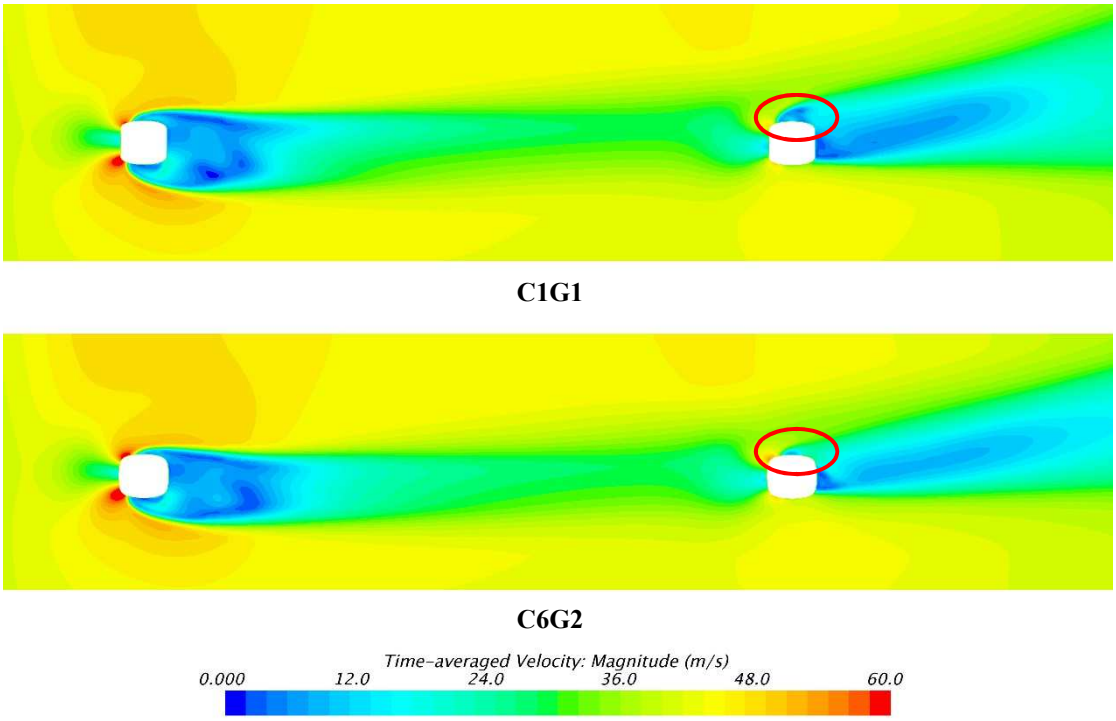

Fig. 25. Time-averaged velocity on z=-0.12 m of Pair 1.

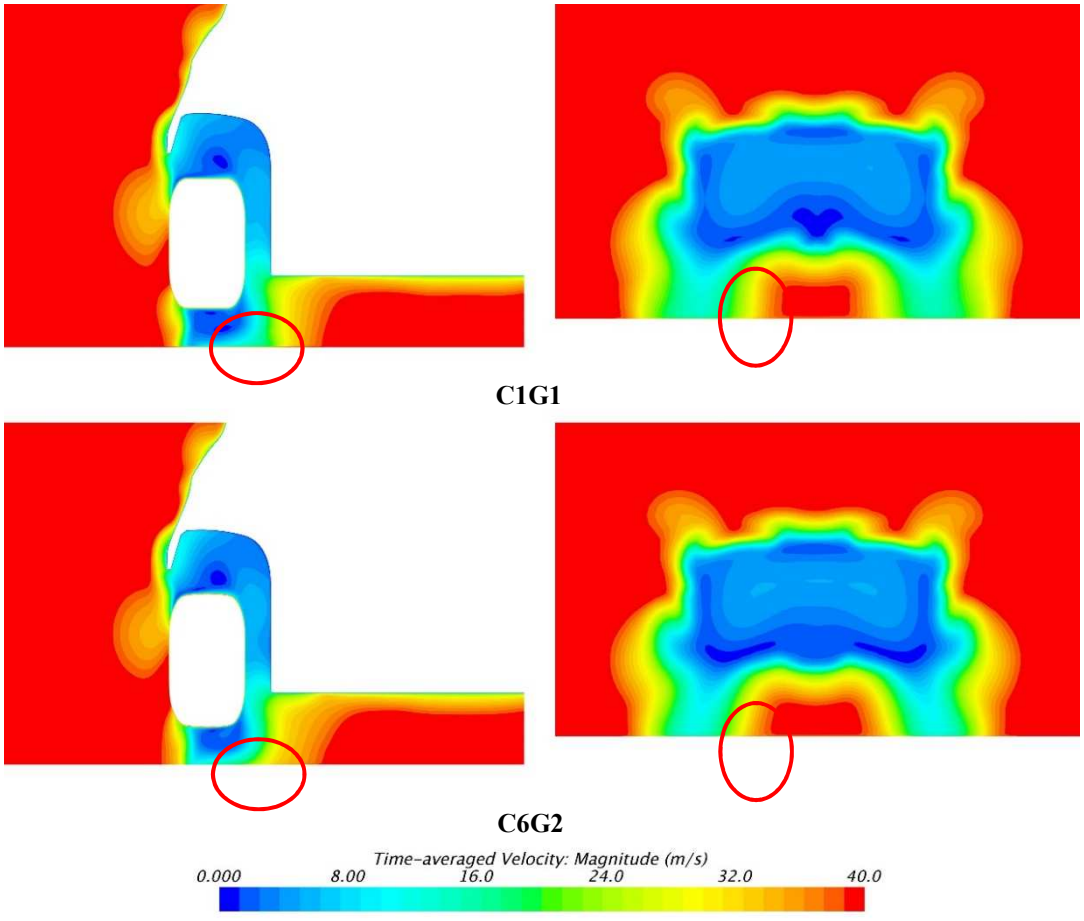

Fig. 26. Time-averaged velocity of Pair 1 (left: 50 mm behind the rear wheel; right: 50 mm behind the body).

Fig. 25 illustrates the time-averaged velocity field around the left wheel patch region. The flow field around the front patch is similar. No significant difference can be observed. However, due to the tiny changes in the contact patch shape, the direction of the front wheel wake is slightly deflected outwards when wheel B is applied. As a result, the oncoming flow of the rear wheel is altered, and the separation on the inner side of the rear patch is suppressed (marked in the red oval).

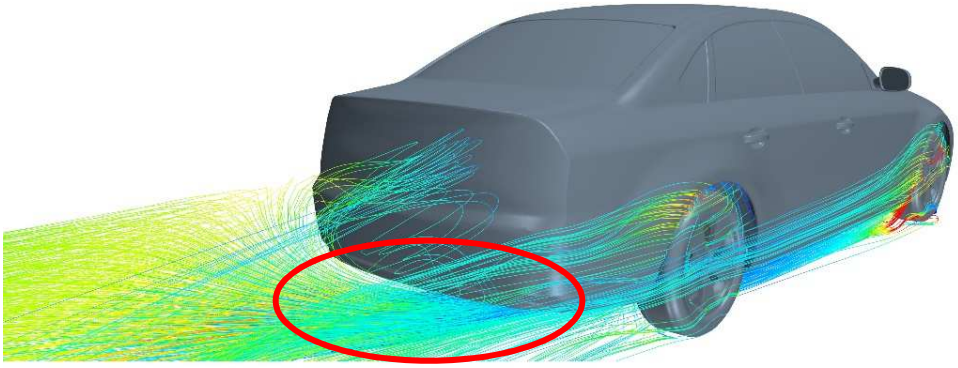

C1G1

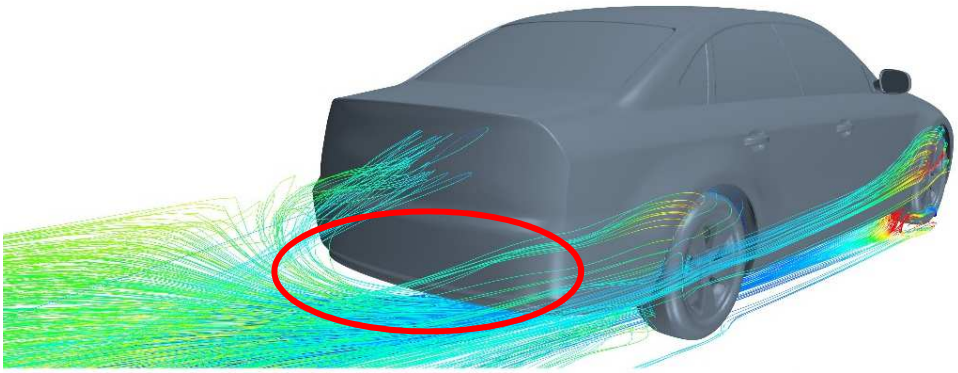

C6G2

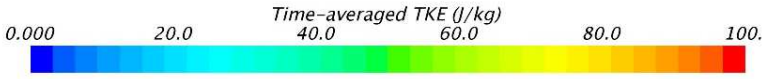

Fig. 27. Streamlines of Pair 1 (colored in TKE).

Velocity on the longitudinal plane 50 mm behind the rear wheel is shown in Fig. 26. It can be seen that around the inner side of the rear patch, the time-averaged velocity increases certainly, especially in the region near the ground. Furthermore, on the longitudinal plane which is 50 mm behind the car body, the velocity increase becomes more notable. It means as the separation is suppressed, the flow rate on the inner side of the patch increases, which can supply the wake and finally reduce total aerodynamic drag.

The streamlines around the rear car are illustrated in Fig. 27, colored in time-averaged turbulent kinetic energy. It can be seen that even though the proportion of the flow passes the inner side of the wheel does not change greatly, the turbulent kinetic energy of the flow in C6G2 significantly decreases, as well as the body wake flow. So in Pair 1, the drag decrease mainly results from the deflected front-wheel wake, which results in the suppressed separation and high-speed inner side flow of the rear patch. This phenomenon also indicates that the diffuser effect under the rear part of the car body can be greatly influenced by the tire tread shape.

The flow field in Pair 2 is more complex than Pair 1. The base C_P of Pair 2 is shown in Fig. 28. It can be seen that similar to Pair 1, C_P of C5G4 is much higher than C5G3, but its magnitude is larger than Pair 1. The main region contributes to the total increment is the same as each other: the central part of the base. It reveals that although the drag difference in Pair 2 is larger than Pair 1, the mechanism of them may be similar.

The time-averaged velocity near the wheel patch region is shown in Fig. 29. On the inner side of the front patch, there is a flow separation in C5G1 but it is suppressed in C5G3. It should be mentioned that this is consistent with the effect of the first critical point in the discussions of Group 2 and Group 3. Due to this condition, the front wake is weakened and deflected outwards significantly in this pair. Furthermore, separations on both sides of the rear patch vanishes and velocity behind the inner side of the rear wheel increases greater than Pair 1, seen in Fig. 30. In summary, the basic reason for drag reduction in Pair 2 is the same as which in Pair 1, but its underbody flow has a higher velocity than Pair 1 so that the total drag reduction is larger, too. Besides, as mentioned above, the effect of the first critical point is similar to the tire tread effect discussed here (accelerate the underbody flow), and the total drag reduction (19 counts) in Pair 2 is approximately equal to the sum of them (9 counts for the first critical point in Group 2 and 12 counts for the tire trend shape in Group 4 Pair 1). So, it is highly possible that these two effects can strengthen each other.

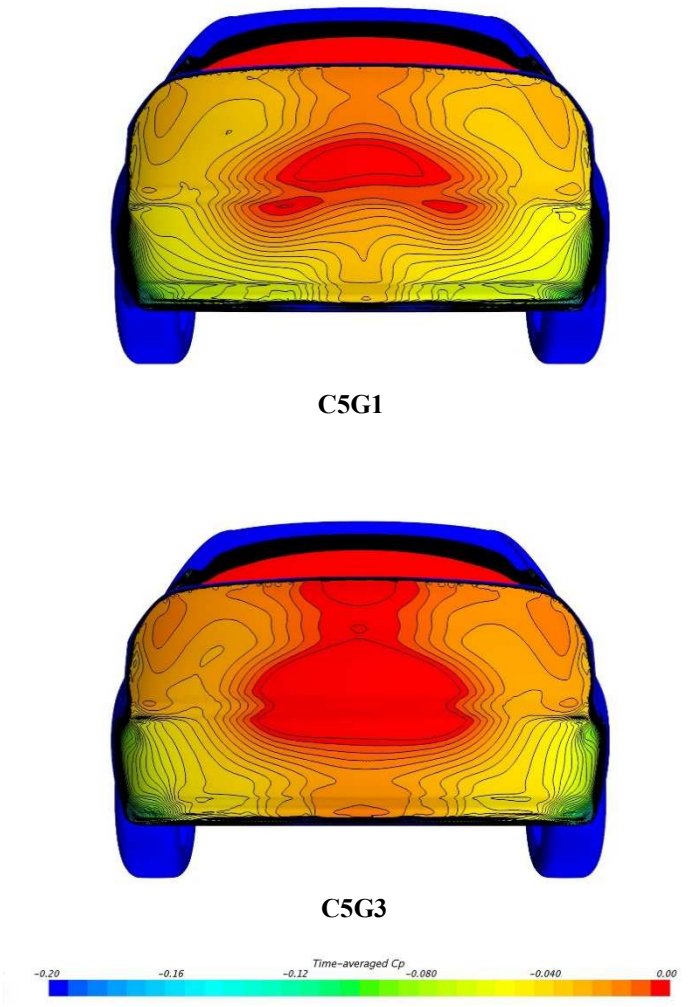

Fig. 28. Base C_P of Pair 2 (upper: C5G1; bottom: C5G3).

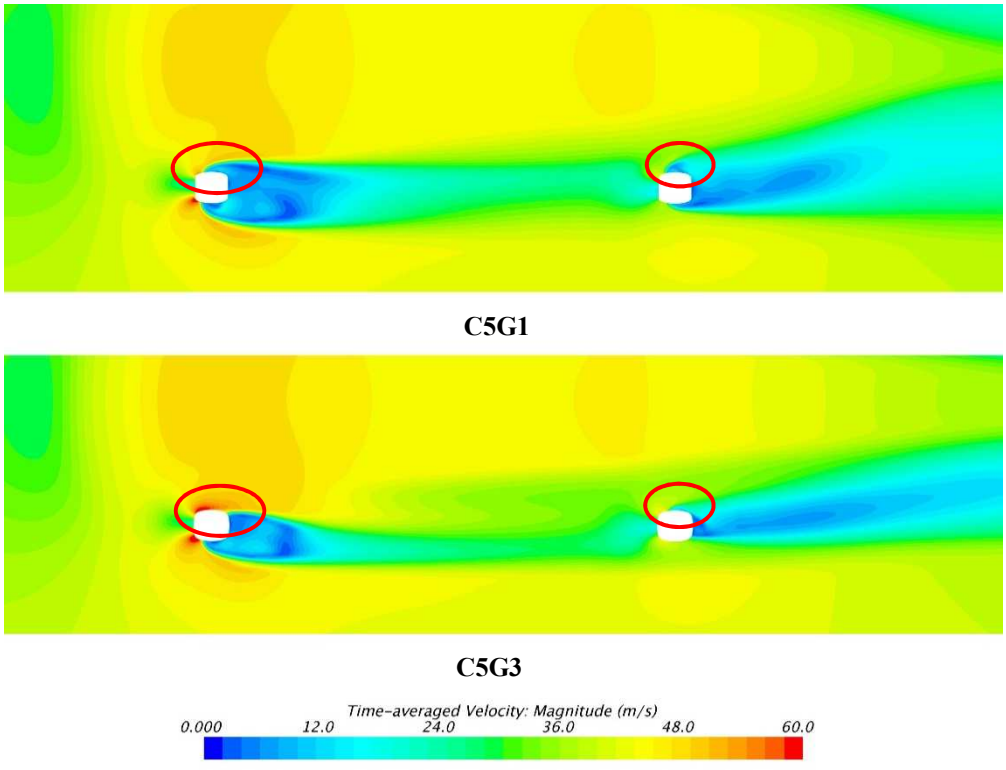

Fig. 29. Time-averaged velocity on z=-0.12 m of Pair 2 (upper: C5G1; bottom: C5G3).

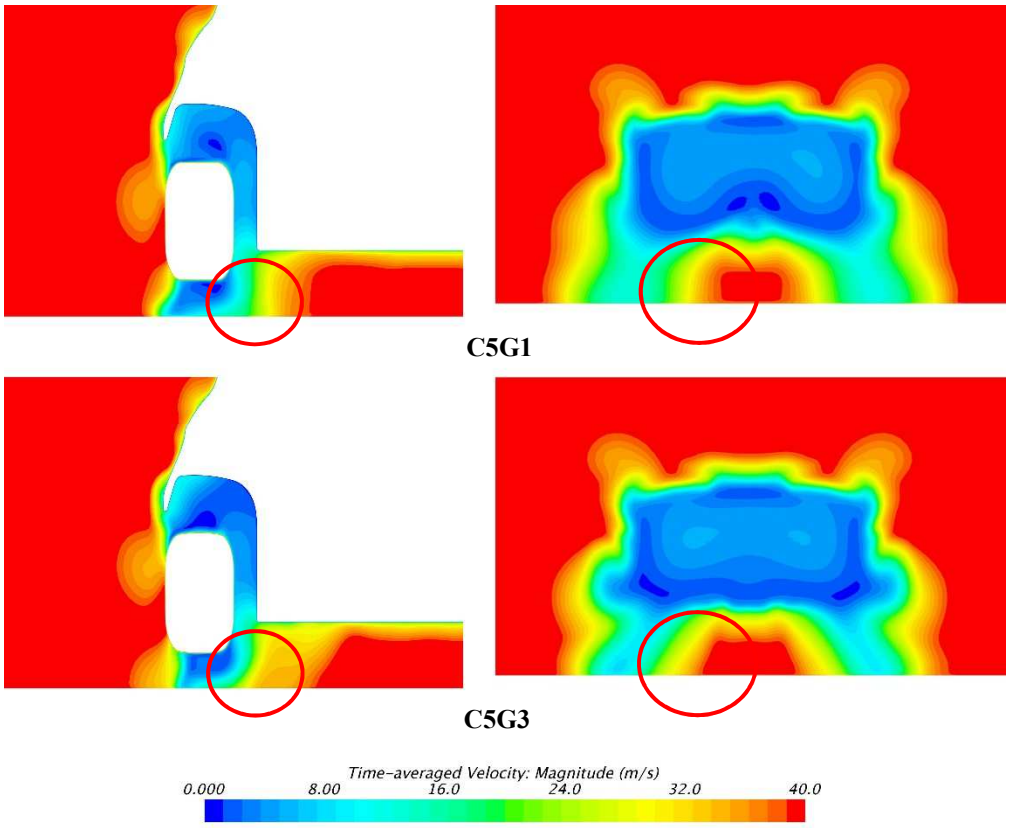

Fig. 30. The time-averaged velocity of Pair 2 (left: 50 mm behind the rear wheel; right: 50 mm behind the body).

Concluding the discussions for Group 4, it is revealed that the aerodynamic features of the DrivAer model are highly sensitive to the tire tread shape. Tiny differences in treads can lead to great differences in the total aerodynamic drag. The main reason is that the contact patch shape may alter the flow direction and change the separation condition around the wheel region, which can alter the flow velocity on the inner side of the rear wheels. While the inner side flow is accelerated, its flow rate will get large and supply extra energy to the trailing vortex of the body, finally weaken the body wake and reduce the total aerodynamic drag. The positions of the critical points are also sensitive to the tread shape. Furthermore, as the effect of tire tread is similar to the critical points, the influence of the latter will also be generated and added to the whole effect if the position of these points is reached coincidentally.

4. Conclusions

In this research three main aspects related to the wheel contact region: contact step height, cut angle, and tire tread shapes are numerically investigated. Main conclusions are listed as follow:

- While the contact step height is not too large, it has little influence on the total aerodynamic force as well as the flow field, except the surface C_P of wheels. Its effect on the global flow field mainly from the separation behind the step but is limited in a certain range.
- When the cut angle increases, two critical points will be reached and the flow separation on the inner and outer side of the front patch will be suppressed respectively. As a result, the overall drag will be reduced and the global flow field will be altered significantly.
- Combining two aspects and keeping the ground clearance unchanged, the main flow features are similar to those when the cut angle is changed only. However, the position of critical points will be altered and the flow field features will be more complex.
- The tire tread shape has a high impact on the aerodynamic coefficients. Tiny changes on the tire tread shape may result in obvious differences in the local flow field (especially rear patch region) and overall drag. Besides, this effect can add to which of the cut angle so huge aerodynamic discrepancies may be obtained.
- Generally speaking, in CFD engineering applications, although there is no such step for the rear wheel, it is still acceptable if adding a step is beneficial to mesh generating unless the surface pressure of wheels is considered important. The cut height and tire tread shape are advised to be set as accurately as possible. As these two parameters will change when the wheels are rotating, it is worth measuring them in the real rotating condition.

Author Contributions

X. Yu planned the scheme, conducted the simulations and wrote the main body of the paper; Q. Jia initiated the project

and analyzed the simulation results; M.M. Rashidi guided this process and made some important revisions. Z. Yang gave the general guidance for this project and added some significant advices. The manuscript was written through the contribution of all authors. All authors discussed the results, reviewed and approved the final version of the manuscript.

Funding

Project 18DZ2273300 is supported by the National Natural Science Foundation of China and Shanghai Key Lab of Vehicle Aerodynamics and Vehicle Thermal Management Systems.

Conflict of Interest

The authors declared no potential conflicts of interest with respect to the research, authorship, and publication of this article.

References

[1] Wickern, G. Zwicker, K and Pfadenhauer, M. Rotating wheels-their impact on wind tunnel test techniques and on vehicle drag results. *SAE Technical Paper*, 970133, 1997.
[2] Yamashita, T. Makihara and T. Saito, Y. et al. Effects of Moving Ground and Rotating Wheels on Aerodynamic Drag of a 2-Box Vehicle. *SAE Technical Paper*, 2018-01-0730, 2018.
[3] Hirose, K. Kawamata, H and Oshima, M. Aerodynamic Sensitivity Analysis of Wheel Shape Factors. *SAE Technical Paper*, 2019-01-0667, 2019.
[4] Brandt, A. Berg, H and Bolzon, A. et al. The Effects of Wheel Design on the Aerodynamic Drag of Passenger Vehicles. *SAE Technical Paper*, 2019-01-0662, 2019.
[5] Fackrell, JE and Harvey, JK. The aerodynamics of an isolated road wheel //*Proceedings of the Second AIAA Symposium of Aerodynamics of Sports and Competition Automobiles*, Los Angleles, California, USA, 11, 1975, 119-125.
[6] Hobeika, T and Sebben, S. Tyre Pattern Features and their Effects on Passenger Vehicle Drag. *SAE Technical Paper*, 2018-01-0710, 2018.
[7] Lew, C. Gopalaswamy, N and Shock, R. et al. Aerodynamic Simulation of a Standalone Rotating Treaded Tire. *SAE Technical Paper*, 2017-01-1551, 2017.
[8] Cogotti, A. Aerodynamic characteristics of car wheels. *INT. J. VEHICLE DESIGN- IMPACT AERODYNAMICS ON VEHICLE DESIGN*, 1983, 173-196.
[9] Sprot, AJ. Sims-Williams, DB and Dominy, RG. The Aerodynamic Characteristics of a Fully Deformable Formula One Wind Tunnel Tyre. *SAE Technical Paper*, 2012-01-1166, 2012.
[10] Guzman, A. Further Analyses on Prediction of Automotive Spinning Wheel Flowfield with Full Width Moving Belt Wind Tunnel Results. *SAE Technical Paper*, 2017-01-1519, 2017.
[11] Diasinos, S. Barber, TJ and Doig, G. The effects of simplifications on isolated wheel aerodynamics. *Journal of Wind Engineering and Industrial Aerodynamics*, 146, 2015, 90-101.
[12] Axon, L. Garry, K and Howell, J. An evaluation of CFD for modelling the flow around stationary and rotating isolated wheels. *SAE Technical Paper*, 980032, 1998.
[13] Mlinaric, P. Investigation of the Influence of Tire Deflection and Tire Contact Patch on CFD Predictions of Aerodynamic Forces on a Passenger Car. *MIRA International Conference on Vehicle Aerodynamics*, 2008.
[14] Heft, AI. Indinger, T and Adams, NA. Introduction of a New Realistic Generic Car Model for Aerodynamic Investigations. *SAE Technical Paper*, 2012-01-0168, 2012.
[15] Forbes, D. Page, G. Passmore, M, et al. A study of computational methods for wake structure and base pressure prediction of a generic SUV model with fixed and rotating wheels. *Proceedings of the Institution of Mechanical Engineers Part D: Journal of Automobile Engineering,* 231(9), 2017, 1222-1238.
[16] Hobeika, T and Sebben, S. CFD investigation on wheel rotation modelling. *Journal of Wind Engineering and Industrial Aerodynamics*, 174, 2018, 241-251.
[17] Shih, TH. Liou, WW. Shabbir, A. Yang, Z, et al. A new k-ε eddy viscosity model for high reynolds number turbulent flows. *Computers & Fluids*, 24(3), 1995, 227-238.
[18] Jia, Q, LI, T and Yang, Z. Influence of Rotating Wheels on Isolated Wheel Aerodynamics. *Journal of Tongji University: Natural Science*, 42(2), 2014, 287.
[19] Söderblom, D. Löfdahl, L. Elofsson, P, et al. Heavy Vehicle Wheel Housing Flows - a Parametric Study. *SAE Technical Paper*, 2009-01-1169, 2009.
[20] Yu, X. Jia, Q. Bao, D, et al. A Comparative Study of Different Wheel Rotating Simulation Methods in Computational Fluid Dynamics. *SAE Technical Paper*, 2018-01-0728, 2018.
[21] Peichl, M. Mack, S. Indinger, T and Decker, F. Numerical Investigation of the Flow Around a Generic Car Using Dynamic Mode Decomposition. *In ASME 2014 4th Joint US-European Fluids Engineering Division Summer Meeting collocated with the ASME 2014 12th International Conference on Nanochannels, Microchannels, and Minichannels*, V01CT17A002-V01CT17A002, 2014.

[22] Yazdani, R. *Steady and Unsteady Numerical Analysis of the DrivAer Model*. Master's Thesis, Chalmers University of Technology, Göteborg, 2015.
[23] Colin, C. A Numerical and Experimental Evaluation of Open Jet Wind Tunnel Interferences using the DrivAer Reference Model. *SAE Technical Paper*, 2016-01-1597, 2016.
[24] John, M. Buga, S and Monti, I. Experimental and Numerical Study of the DrivAer Model Aerodynamics. *SAE Technical Paper*, 2018-01-0741, 2018.

ORCID iD

Xiaoyan Yu https://orcid.org/0000-0001-8263-3589
Mohammad Mehdi Rashidi https://orcid.org/0000-0002-6309-8688